10th International Conference on Math. Modelling of Weld Phenomena, Seggau, Sept. 2012, Eds. C. Sommitsch and N. Enzinger, TU-Graz, 2013, p. 501-519.

SIMULATION OF WELDING STRESSES FOR FATIGUE DESIGN OF WELDED TUBULAR CONNECTIONS

C. ACEVEDO*, J. M. DREZET** and A. NUSSBAUMER*

*ICOM Steel Structures Laboratory, EPFL Lausanne (Switzerland)
**LSMX Computational Materials Laboratory, EPFL Lausanne (Switzerland)

ABSTRACT

This paper presents a 3D thermo-mechanical model of arc-welding applied to tubular K-joints susceptible to fatigue cracking. The 3D torch trajectory is reproduced to simulate both temperatures and stresses during welding and ultimately the 3D residual stress distribution after cooling. The influence of latent heat, of the increase of thermal conductivity to simulate the fluid convection within the weld pool, the activation of finite elements to simulate the use of filler wire and the number of passes on as-welded residual stresses is assessed using ABAQUS. Actions taken to simplify the problem and reduce the computation time are presented and discussed. Comparisons of fusion zones obtained numerically and using optical macrographs as well as comparisons between calculated and measured residual stresses are presented. This numerical analysis highlights high tensile residual stresses occurring at the gap zone which is the most critical location where fatigue cracks initiate and propagate in tubular bridge K-joints.

1. INTRODUCTION

During welding, non-uniform thermally induced deformations lead to plastic strains and residual stresses or distortions. Residual stresses induced by welding have three main origins [1]. Firstly, the gradient of temperature and the non-uniform cooling in the welded area induce plastic deformations and hence residual stresses. These stresses are called thermal residual stresses. Secondly, mechanical effects such as clamping, restraining, misfits, etc. participate in the creation of residual stresses. These effects are also related to the drop of mechanical properties, such as the Young's modulus and the yield stress, at high temperatures. Thirdly, solid phase transformations that imply the local transformation of a microstructure into another one depending of the welding thermal cycle lead to additional residual stresses, called transformation residual stresses. This phenomenon is mainly due to volumetric changes and transformation plasticity.

In mild steels, thermal residual stresses are usually large tensile stresses whereas transformation residual stresses are compressive stresses in the weld area. The sign of mechanical residual stresses depend on the clamping conditions. High tensile residual stresses have a detrimental effect, among others, on the fatigue strength [2] of welded structures.

For the construction of tubular truss bridges, K-shape joints with non-overlapping tube members are often chosen to minimize the number of joints in bridges. K-joints and especially the non-overlapping gap region are the areas of the bridge most susceptible to

fatigue loading. High tensile residual stresses are combined with high applied stress concentrations and welding imperfections.

To design these bridge structures against fatigue, an accurate and reliable estimate of welding and residual stresses is crucial. However, accurate finite element simulation of a non-linear transient problem such as welding (non-linear temperature-dependent material properties, the weld pool moving with the weld source, etc.) is quite challenging and computationally demanding. In addition, the shape of the joints leads to even more geometric complexity. That is the reason why several aspects of the problem have to be idealized and/or simplified while maintaining an accurate result by comparison with measurements.

To optimize the quality of numerical results, one has to focus on modelling aspects that most influence the magnitude and distribution of residual stresses [3, 4]:

- Geometry of the joint (shape, dimensions, thicknesses, and position of the welds) and restraint conditions related to this geometry.
- Temperature dependent material properties (Young's modulus E, thermal expansion coefficient α, yield behaviour, etc.).
- Heat distribution, number of weld passes and welding sequence.

Two other aspects can be considered as significant in general but they are shown to be negligible in our case:

- Phase transformation from austenite to ferrite-perlite may lead to compressive stresses reducing large tensile residual stresses. In the case of mild steels, this phenomenon is negligible and transformation residual stresses are not taken into account.
- Applied external loads can either increase or decrease residual stresses [4, 5]. Residual stresses are reduced so that the maximum combined stress is equal to the cyclic yield limit that can be lower than the static yield limit. In case of high stress multiaxiality and/or high notch effect, the relevant yield limit is increased so that there is no or slightly residual stress reduction. Large-scale K-joints with large wall thicknesses ($T \geq 20$ mm) and welding imperfections belong to such welded components for which the applied loads have almost no influence on the residual stress distribution.

In the present work, a 3D thermo-mechanical analysis is chosen to simulate the arc-welding process. Main assumptions and simplifications of the model are discussed. As stated above, a particular attention is paid to the geometry, material properties and heat distribution. The 3D complex geometry of K-joints with their welds is modelled and compared to real-scanned geometry. The heat source is adapted so that simulated fusion zones match the ones obtained using optical macrographs. The validation of the model in terms of residual stresses compared with stresses measured using neutron diffraction is reported in [6]. Following this validation, a sensitivity study is performed on a reduced part of the K-joint welding sequence. The effects of the solid-liquid latent heat, the increase of the thermal conductivity to simulate fluid flow within the weld pool, the finite element

activation to simulate the use of a filler wire and the number of simulated passes are investigated.

2. METHODOLOGY AND ASSUMPTIONS

The Metal Active Gas MAG process combined with a flux-cored electrode is adopted to weld non-alloyed steel S355 tubular hollow sections. Several physical phenomena occur during arc welding: arc and weld pool physics, heat transfer, metallurgical phenomena and stress-strain generation. Lindgren [18, 27] and Dong [26] proposed several recommendations to simulate the welding efficiently, indicating which phenomena are of low importance in determining the residual stress state.

2.1. SIMPLIFICATION OF ARC AND WELD POOL PHYSICS

The electric current passing through the gas of the welding arc is transformed into heat. Only part of the energy produced by the arc is absorbed by the metal to create a molten pool [7, 8, 9]. It has been demonstrated that convective flow in the weld pool has a strong influence on the profile of the fusion line (size, shape and penetration of the weld pool) and hence on the residual stress distribution. The fluid convection in the liquid pool can be successfully computed with finite elements [10]. However, to avoid modelling the complex arc and weld pool phenomena, phenomenological heat source models are often preferred [11]. In the present model, arc and weld pool physics are not considered and an equivalent heat source is used to reproduce the weld fusion profile. The characteristics of the heat source, i.e. its intensity but also its temporal and spatial distribution, are determined by comparing the calculated size and shape of the weld fusion zone with the one obtained by optical micrographic inspection [12].

2.2. METALLURGICAL COUPLING

The heat-affected tone (HAZ), where fatigue cracks usually initiate, is not melted but transformed at high temperature. The ferrito-pearlitic microstructure of welded components in S355 steel is partially transformed into austenitic microstructure for temperatures above the arrest transformation point A_{c1}, and entirely for temperatures above the arrest transformation point A_{c3}. The austenite formed in the HAZ after solidification is then transformed during cooling into ferrite, bainite, pearlite and martensite depending on the welding thermal cycle, the size of the austenite, the cooling time, and the steel composition.

Martensitic transformation is well known to imply a significant volume increase along with transformation plasticity, e.g. plastic strains induced by metallurgical transformation [29]. Jones and al. have already shown in 1977 that phase transformation influences the residual stress distribution [28]. Phase transformation may decrease drastically the tensile residual stress intensity, sometimes up to negative values [13, 14].

The fraction of the hard microstructure of martensite is studied by Vickers hardness testing (EN ISO specification 6507-1 [15]) on a cross-section at the weld area. Hardness was measured at 55 points in the cross-section using a 1 kg-force during 16 seconds. Hardness values vary from 180 to 232 HV in the HAZ region. These Vickers hardness ranges correspond to a combination of ferrite, bainite and pearlite microstructures with potential traces of martensite [16] for non- or low-alloyed steel.

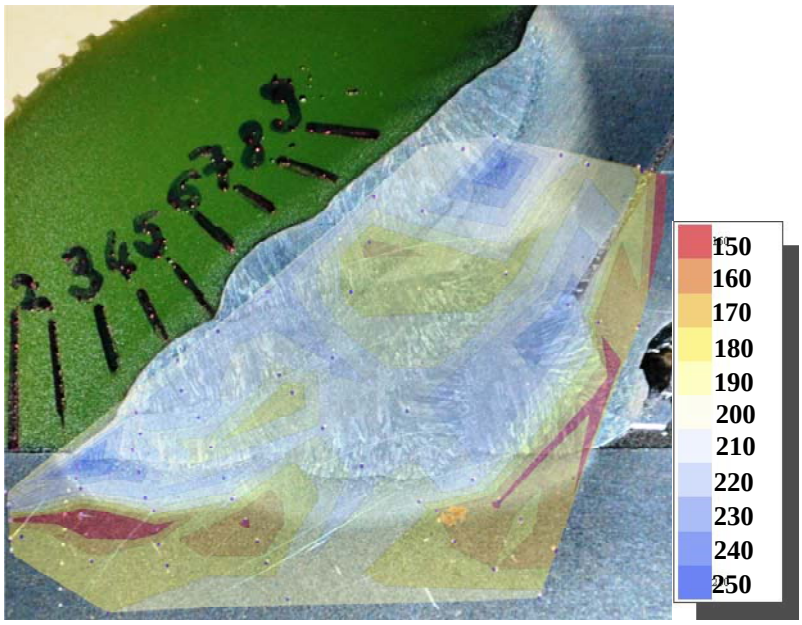

Fig. 1 Map of Vickers hardness values (measurement points are represented by dots).

Therefore, martensitic transformation is considered as low and may be neglected for the residual stress analysis thus avoiding the necessity of coupling the thermo-mechanical approach with a metallurgical model. Only the heat released by fusion and solidification, i.e. the solidification latent heat, is taken into account in the thermal cycle.

2.3. THERMO-MECHANICAL ANALYSIS

With the previous simplifications and assumptions, the problem is reduced to a one-way coupled thermo-mechanical analysis (two consecutive steps) as presented in Fig.2. First, a 3D transient thermal analysis is performed to determine the temperature field history throughout the computation domain, which comprises two braces and a section of the chord. Second, the stress-strain problem is solved using the temperature field as input. Heat dissipation by mechanical work is ignored.

The thermal analysis consists in solving the heat conduction problem considering heat losses by radiation and convection and heat introduced by the weld source. The latent heat induced by melting and solidification is also included. To account for the fluid flow within the fusion bed, the thermal conductivity is artificially increased above the melting temperature of the steel. Since the density magnitude of this carbon steel does only weakly depend on temperature, it is taken as a constant and hence does not appear in Figure 2. For the mechanical analysis, the material behavior is formulated as elastic-plastic with a linear isotropic hardening. All numerical analyses are performed using ABAQUS standard 2011 [17]

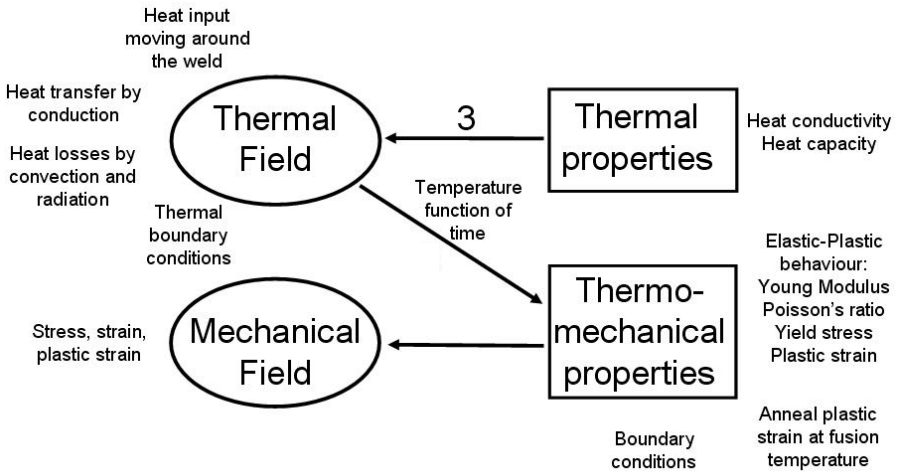

Fig. 2 The thermo-mechanical analysis adapted from Lindgren [18].

3. K-JOINT LUMPED PASS MODEL

The model used to simulate the stress generation in a tubular K-joint by reproducing the entire welding sequence is presented hereafter. This model is called Lumped Pass Model and the resulting residual stress distribution has been validated with measurement values obtained using neutron diffraction and published elsewhere [6, 12]. The features of the lumped pass model are recalled hereafter as this model will be the basis for the sensitivity analysis.

3.1. GEOMETRY OF THE K-JOINT

The K-joint considered here is composed of two brace branches welded onto a chord member. The chord is 168.3 mm in diameter with 20 mm wall thickness. The braces are 88.9 mm in diameter with 8 mm wall thickness. The brace angle is 60° and the gap dimension is

51 mm. These dimensions are akin to the one used in real bridge construction. Dimensions of the weld are taken from [19] who found out a proportional relation between weld widths and brace wall thickness. Backing rings are placed inside the brace members in order to facilitate the welding of the braces onto the chord but they do not affect the fatigue resistance of the joint [20] and hence are not introduced in the numerical model. As shown in Fig.3, seven weld passes are needed to ensure a full penetration weld using a flux cored arc welding. For each weld pass, a welding sequence of four steps is done as depicted in Fig.4. To minimize the computation time, the seven weld passes are lumped into a single pass as will be detailed hereafter. The complex shape of the weld is defined numerically by equations representing the brace-chord, the weld-brace and the weld-chord intersections in 3D. The finite element computation domain is made of 25544 elements and 30833 nodes. It is shown in fig. 4b. Element size and type of interpolation have been optimised to get acceptable CPU times [12].

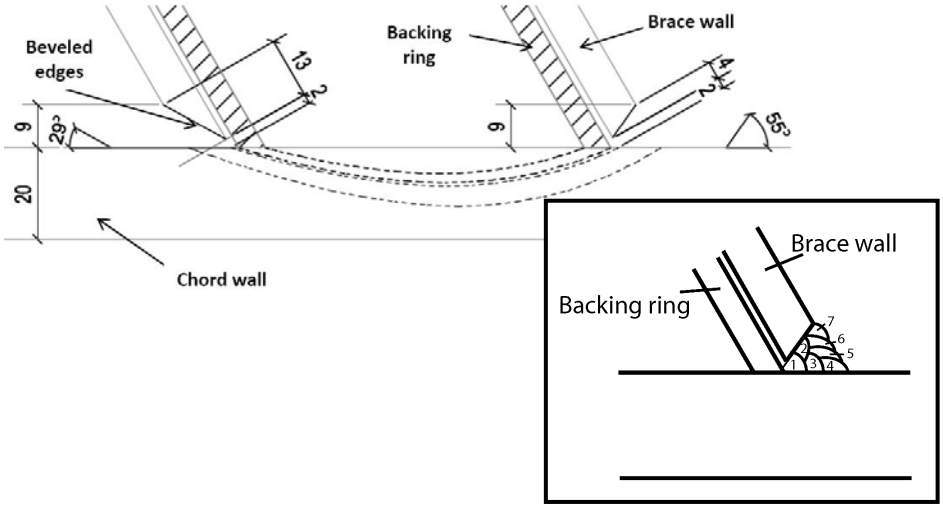

Fig. 3 Cross section of a brace-chord joint: brace cut end with bevel edges and 7 welding passes forming the full penetration weld (dimensions in mm).

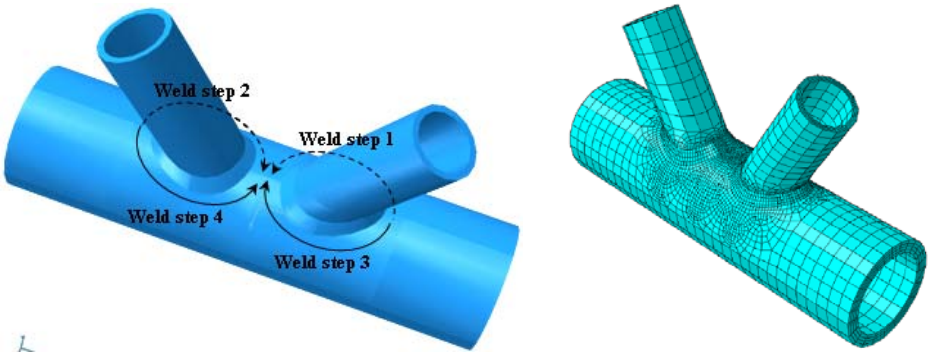

Fig. 4 Four steps of the welding sequence applied for each of the 7 passes (left) and FE mesh (right).

3.2. TEMPERATURE-DEPENDENT MATERIAL PROPERTIES

The non-linear heat conduction equation [12] is solved with temperature-dependent thermal properties. Their values are given in Table 1. A constant density of 7850 kg/m^3 is taken. The latent heat L is rejected during solidification and absorbed during fusion. It is included in the model using an increases specific heat between the solidus (1465°C) and liquidus (1544°C) temperatures of the alloy. A value of 247000 J/kg is used [21]. At temperatures greater than the liquidus temperature (1544°C), convective flows accelerate the weld pool temperature homogenization. To take into account that particular aspect, the conductivity in the liquid, i.e. at temperatures higher than 1544°C, is artificially increased to three times its value at the solidus temperature [11, 22, 23] and kept constant.

Table 1 Thermal conductivity k (W.m^{-1}.°C^{-1}) and specific heat C (J.kg^{-1}.°C^{-1}) for the steel grade S355 taken from the Eurocode 3 Part1-2 [24].

T (°C)	20	100	200	300	400	500	600	650	700	735	750	800	900	1200
k	53.3	50.7	47.3	44	40.7	37.4	34		30.7			27.3	27.3	27.3
C	440	488	530	565	606	667	760	814	1008	5000	1483	803	650	650

Table 2 Young's modulus E (10^3 MPa) [24], Poisson's ratio ν [25] and the thermal expansion α (10^{-6}/°C) [25], for the steel grade S355.

T (°C)	20	100	200	300	500	600	700	800	900	1000	1465	1544
E	210	210	189	168	126	65.1	27.3	18.9	14.2	13	10	1
ν	0.296	0.311	0.33	0.349	0.386	0.405	0.423	0.442	0.461	0.48	0.48	0.48
α	11.7	11.7	11.8	12.2	13.2	13.6	13.8	-	-	-	15	-

Table 3 Stress evolution (in MPa) as a function of plastic strain (0, 10 or 100%) and temperature [25].

T (°C)	20	100	200	300	500	600	700	800	900	1000	1465	1544
fy (0%)	345	332	308	276	186	128	69	64	46	11		
fy (10%)	423	410	386	342	231	163	96	84	61	21		
fy (100%)											1	0.1

Temperature-dependent mechanical properties are used in the calculations of the residual stress build-up. A linear isotropic strain hardening law is used to model the steel behaviour. Kinematic and visco-plastic effects are not taken into account. The thermo-elastic behaviour is defined by the Young's modulus E, the Poisson's ratio ν and the thermal expansion coefficient α. They are given in Table 2 as a function of temperature. The linear isotropic plastic behaviour is defined by the yield stress and the stress value for a plastic strain of 10% as a function of temperature (Table 3). The *ANNEAL TEMPERATURE option in ABAQUS is set to the solidus temperature to avoid the accumulation of plastic strains when the material is in the semi-solid or liquid state.

3.3. HEAT DISTRIBUTION

Arc welding is performed with a welding current of 270 A, an arc voltage of 30 V and an efficiency estimated to 0.73 according to the welding procedure specifications. The degree of efficiency corresponds to the part of heat input effectively used to create the weld; the rest is lost by convection and radiation. The welding torch is moved with a travel speed of 5.5 mm/s. To comply with energy balance in merging the seven weld passes into one, the total energy input is kept identical (26, 18). This energy, called Q hereafter, is defined as follows for the 7 pass-welding:

$$Q = 7 \times \eta.U.I \times \frac{d}{v} \quad (1)$$

where Q is the energy input (J), η is the welding efficiency, U is the voltage (A), I is the current of the arc welding, d is the travel distance of the torch (mm) for one pass, i.e. for the

four sequences depicted in fig. 4, and v is the welding speed (mm/s). In our case, Q is equal to 41.5 kJ welding time of 1s. In the lumped pass model, the total energy input is conserved by introducing in one lumped pass the equivalent electrical power, 7.ηUI, and by keeping the same welding distance d and speed v. To approximate the arc-welding heat source, a spherical heat source model is chosen with a radius of 15 mm as shown in Figure 5. In comparison with the Goldak heat source model [11], which requires to experimentally identifying several dimensional parameters describing the ellipsoid geometry, the spherical model just requires to determine the radius r (easily measured on the welded sample).

As the centre of the sphere moves on the very surface of the weld, the equivalent power 7.ηUI is uniformly distributed within half of the sphere thus yielding a volumetric power of 5.87 W/mm^3.

Fig. 5: Schematic representation of the spherical heat source used in the lumped model.

Each of the welding sequence reported in Fig.4 lasts 25 s and is followed by a cooling step of 125 s. The final welding sequence is followed by a longer cooling step of 9000 s. Note that there was a preheating up to 100°C and that the interpass temperature was kept bellow 250°C (usually between 100°C and 200°C).

4. SENSITIVITY STUDY ON A REDUCED WELDING SEQUENCE

In order to assess the influence of several assumptions in developing the thermo-mechanical model, a sensitivity study is performed using the K-joint geometry presented above but with a welding sequence reduced to the welding sequence 1 shown in Fig.4. The study aims at identifying the most accurate and suitable model to evaluate as-welded residual stresses in an efficient manner. The effects of the latent heat, the increased thermal conductivity to simulate the fluid flow within the molten zone, the weld metal deposition using the activation of finite elements and the number of simulated passes are investigated.

4.1. METHODOLOGY

Fig. 6 represents a sketch of the six sensitivity cases that are based on the lumped pass model presented before and reduced to the first welding sequence (model 0). One feature is changed at a time to be efficient when comparing the results with the reference case.

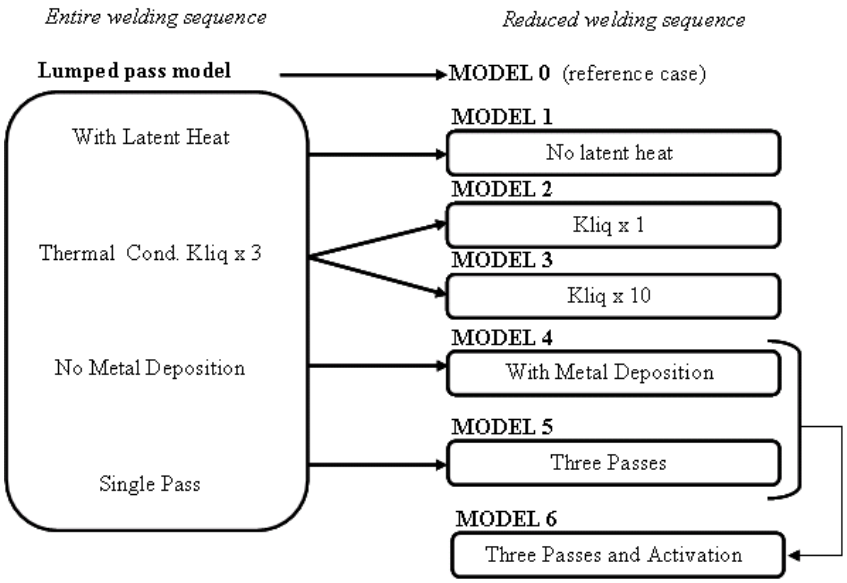

Fig. 6: Sketch of the six sensitivity cases to be compared with the lump pass model.

4.2. EFFECT OF LATENT HEAT

Model 1 is similar to the reference case except that latent heat is not taken into account.

4.3. EFFECT OF AN ARTIFICIALLY INCREASED THERMAL CONDUCTIVITY

In model 2, the thermal conductivity is not increased at temperatures higher than the solidus temperature but remains equal to its value at the solidus temperature, i.e. to 27.3 W/mK. In model 3, the thermal conductivity is linearly increased from 27.3 W/mK at the solidus temperature to 273 W/mK (10 times) at the liquidus temperature.

4.4. EFFECT OF THE WELD ELEMENT ACTIVATION

Model 4 is identical to model 0 but with a progressive activation of the weld finite elements to model the deposition of the filler metal. The weld area is divided into a series of consecutive blocks. The on-going welding of the brace onto the chord is simulated conjointly with the movement of the heat source. The activation of elements is done in 13 successive steps, in each step the weld block is activated when the spherical heat source is touching it. The heat distribution remains the same as in case 0. Before starting welding, a

gap is present between the brace and the chord as in reality (see fig. 7). As welding progresses, sets of elements (or blocks) are included in the model thus modelling the joining between the brace and the chord from a mechanical point of view similarly to a zipper closing a garment. Blocks are activated with an initial temperature of 20°C and the spatial and temporal heat distribution remains identical to model 0.

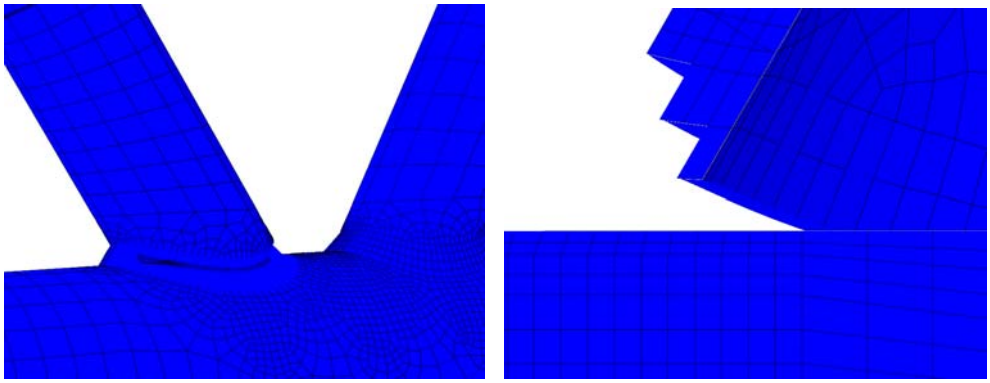

Fig. 7: View of case 4 at the beginning of computation when weld elements are not yet activated.

4.5. EFFECT OF THE NUMBER OF PASSES

In model 5, there is no activation of finite element blocks meaning that all the elements are in the model from the beginning of the welding. Three weld passes are simulated instead of one lumped pass. The weld area is divided in the 1st equivalent pass area, the 2nd equivalent pass area and the 3rd equivalent pass area. Each pass area is divided in a series of consecutive blocks. Following the movement of the torch, the heat is brought within the element blocks forming the 1st equivalent pass, the 2nd equivalent pass and the 3rd equivalent pass that appear in fig. 14 in the results section. To balance the total heat input, the equivalent power, 7.ηUI, is divided by three and uniformly distributed within the volume of each block thus yielding a volumetric heat input around 24 W/mm^3 for each of the three passes.

4.6. THREE PASSES WITH ELEMENT ACTIVATION

Finally, model 6 is similar to model 5 except that the blocks forming the 1st equivalent pass, the 2nd equivalent pass and the 3rd equivalent pass are activated one by one when they are heating. This case is the closest to reality except for the number of passes.

5. VALIDATION WITH EXPERIMENTS AND SENSITIVITY RESULTS

In this section, the results obtained with the lumped pass model are compared with optical micrographs and residual stresses measured with the help of neutron diffraction. Then the results of the sensitivity analysis are compared and discussed.

To ease the comparisons, only two features that appear to be essential for the quality of the modelling are retained: the weld fusion profile at the end of the last welding sequence, i.e. right before starting the cooling step, and the distribution of the transverse stress component after complete cooling as a function of depth in the weld toe area which is the zone prone to cracking.

5.1. VALIDATION OF THE LUMPED PASS MODEL

Fig. 8 shows the comparison of the fusion zone with the lumped pass model and fig. 9 the comparison with the transverse stresses measured using neutron diffraction. Further details on the validation of this model can be found in [6]. Fusion zones are well reproduced by the numerical model on the chord side but not perfectly on the brace side. In the simulation, he liquid weld bead is larger than in reality on the brace side and not perfectly fitting the weld toe on the chord side. This is due to the shape of the spherical heat source. Since fatigue cracks initiate on the chord side, the brace side estimate is of less importance. Although the lumped pass model lies on many assumptions, it appears to be able to correctly reproduce the stress build up during welding (fig.9). The aim of the sensitive analysis is to understand why.

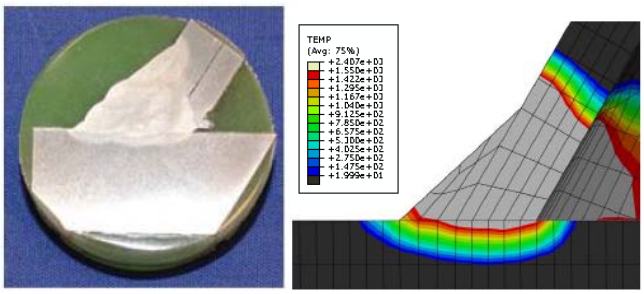

Fig. 8: Comparison of the fusion zone with predictions using the lumped pass model [6].

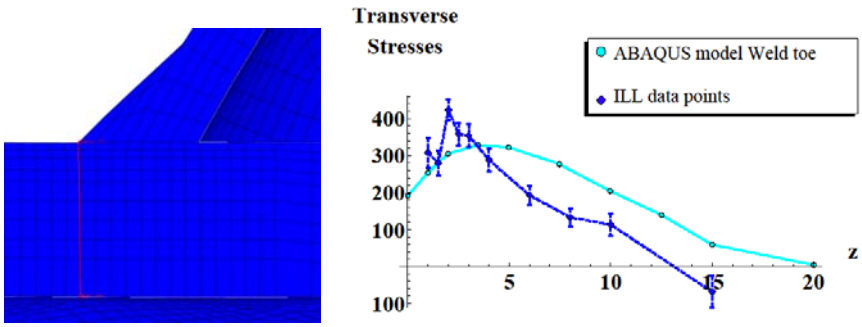

Fig. 9: Path along which the transverse stress profiles are compared (left) and comparison with neutron diffraction measurements (right) [6]. Stresses are given in MPa and depth z in mm.

5.2. EFFECT OF LATENT HEAT AND THERMAL CONDUCTIVITY IN THE LIQUID

Models 1 to 3 yield very similar results compared to the reference case in terms of temperature, fusion zone and transverse stresses as shown in fig. 10. Including latent heat does not affect the results. Therefore this high non-linearity can be skipped in such calculations.

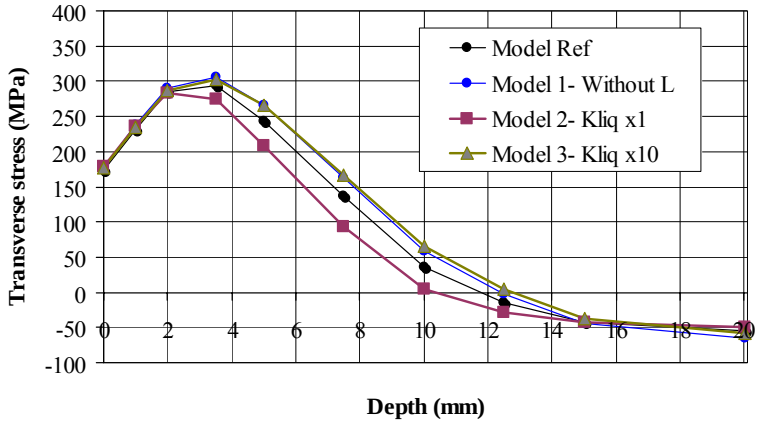

Fig. 10: transverse stress as a function of depth for models 0 to 3.

5.3. EFFECT OF WELD ELEMENTS ACTIVATION

Model 4 which features a progressive activation of finite elements to simulate the on-going welding of the brace onto the chord as the heat source moves, yields a fusion zone that is very similar to the one calculated using the reference case, as shown in fig. 11 (comparison

Model 0 and Model 4). Albeit, model 4 predicts transverse stresses that are higher by more or less 50 MPa compared to case 0 (cf. fig. 12). This is explained by the fact that the gap between brace and chord is free to increase or reduce in front of the weld torch. As shown in figure 13, both sides of the weld tend to separate before the source is heating them. Welding has to overcome this tendency to properly join them and therefore residual stresses are higher owing to the "zip effect". Note that the higher stresses, over 350 MPa that model 4 leaded to, are closer to the measured values of a four welding sequence (Fig. 9).

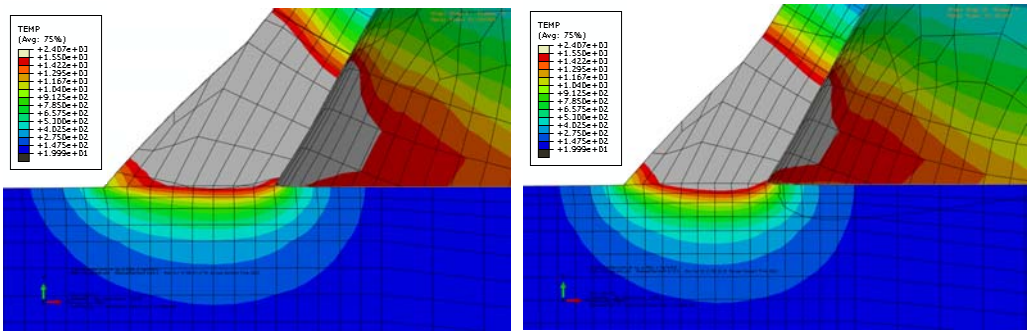

Fig. 11: Fusion zone at the end of welding sequence 1 for models 0 (left) and 4 (right).

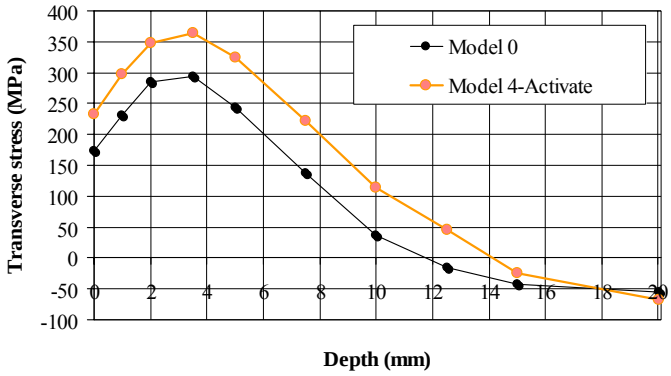

Fig. 12: Transverse stress as a function of depth for models 0 and 4.

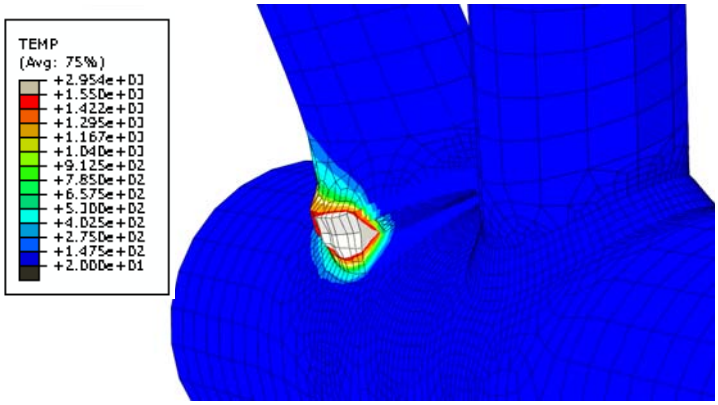

Fig. 13: Opening of the lips in front of the weld under the torch and closure of the lips by the activation of elements ("zip effect").

5.4. EFFECT OF THE NUMBER OF PASSES

Sensitivity analysis devoted to the influence of the number of passes on the residual stress estimation concluded that a three-pass model is sufficient to describe the residual stress distributions of a multiple-pass weld according to [26]. Lindgren [18] did not propose a number of weld passes but underlined the fact that merging weld passes into one equivalent pass by keeping the total heat input gives the most accurate results. The results given by model 5 follow the same trend. They are very similar to case 0 (cf. fig. 14 and 15) provided special care is given to the spatial distribution of the heat input for each pass while keeping the whole heat input constant.

Note that by combining the fusion zones from the three passes of Fig. 14, one get a fusion line on the brace side which is in good agreement with the micrographs (see Fig. 8). The multipass model improves the fusion zone definition by comparison with model case 0.

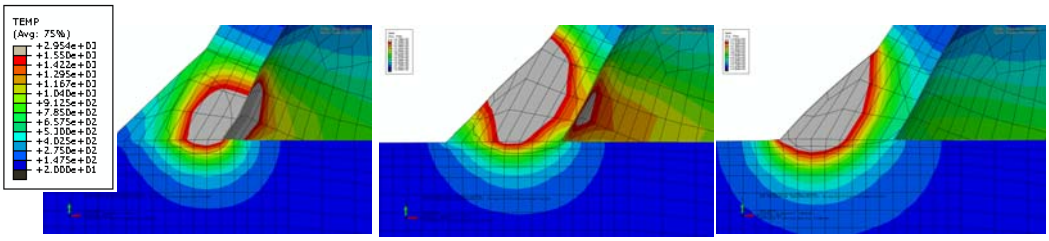

Fig. 14: fusion zone at the end of each pass for model 5 (similar legend than in Fig.11).

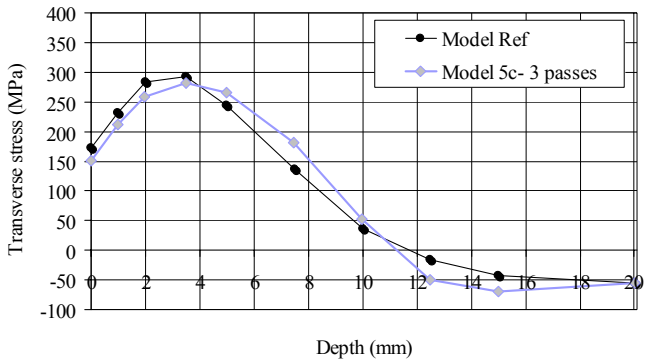

Fig. 15: transverse stress as a function of depth for models 0 and 5.

5.5. EFFECT OF ELEMENT ACTIVATION WITH THREE PASSES

Model 6 is the one that is closest to reality as it simulates more than one pass and it takes into account the zip effect by activating elements as the torch moves. Nevertheless, the model is rather complex notably the definition of the elements to be activated and CPU time intensive. Fig. 16 and 17 reveal that the results agree in an acceptable extent with the results coming from model 0 (reduced lumped pass model). The reason is that the zip effect indeed increases the stresses but only during the first pass. This effect disappears with the following passes thus justifying the fact that it can be ignored.

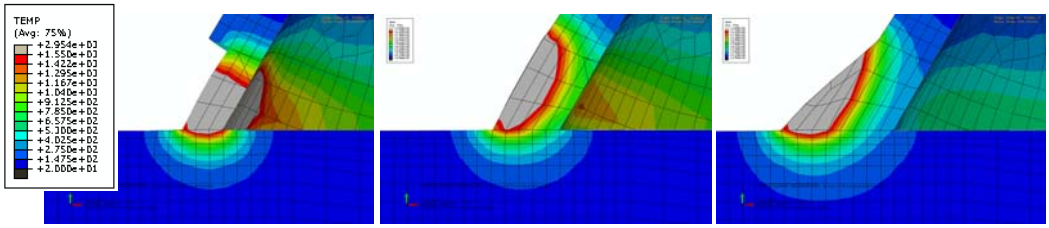

Fig. 16: fusion zone at the end of each pass for model 6 (similar legend than in Fig.11).

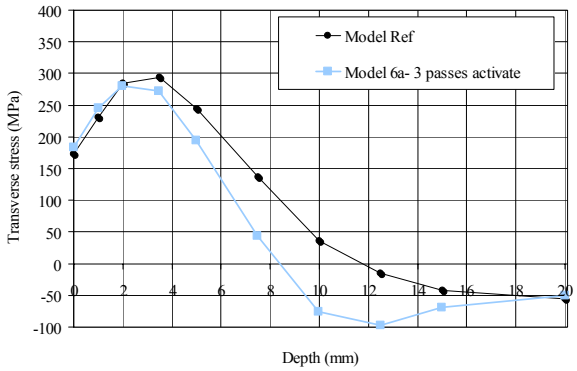

Fig. 17: transverse stress as a function of depth for cases 0 and 6.

6. CONCLUSION

The 3D thermo-mechanical model of arc-welding presented here is based on a lumped pass approach. It has been validated with both the fusion zone profile and the measured transverse stress distribution in the gap zone which is the most critical location where fatigue cracks initiate and propagate in tubular bridge K-joints. A sensitivity analysis is carried out on a reduced welding sequence. The sensitivity analysis shows that the influence of the thermal conductivity in the liquid and the latent heat is minor. On the other hand, the zip effect due to element activation gives higher stresses but this effect is present only during the first pass. It is worth noting that the reduced welding sequence (used in models 0 to 6) may not completely take into account the restraining effects due to the three other welding sequences (lumped model).

As a conclusion, provided both metallurgical transformations and visco-plastic effects can be ignored, the lumped pass model without any element activation appears to be realistic enough to simulate the stress generation during arc-welding. Conserving the total heat input when defining the heat distribution is of prime importance.

7. ACKNOWLEDGMENTS

The research presented herein was supported by the Swiss National Science Foundation (SNF). The authors would like to thank Dr. A. Evans and Dr. D.J. Hughes for their help during neutron-diffraction experiments at the Paul Scherrer Institute (POLDI), Villigen Switzerland and at the Institute Laue-Langevin (SALSA), Grenoble, France, respectively.

REFERENCES

[1] J. LU, J. F. FLAVENOT and Lieurade, H. LIEURADE: *Intégration de la notion des contraintes résiduelles dans les bureaux d'étude*, 1991.

[2] C. ACEVEDO, A. NUSSBAUMER: 'Effect of tensile residual stresses on fatigue crack growth and **S**–**N** curves in tubular joints loaded in compression', *International Journal of Fatigue 36,*. 171-180, 2012.

[3] P. WITHERS, M. TURSKI, L. EDWARDS, P. BOUCHARD AND D. BUTTLE: 'Recent advances in residual stress measurement', *International Journal of Pressure Vessels and Piping 85(3),*. 118-127, 2008.

[4] J. KREBS, M. KASSER: 'Influence of welding residual stresses on fatigue design of welded joints and components', *Welding in the world 51(7/8), 2007*.

[5] T. NITSCHKE-PAGEL: 'Eigenspannungen und Schwingfestigkeitsverhalten geschweisster Feinkorstähle (Residual stress and fatigue behaviour of welded fine grain steels)', Diss. Tech. Univ. Braunsweig, 1994.

[6] C. ACEVEDO, J.-M. DREZET and A. NUSSBAUMER: 'Numerical modelling and experimental investigation on welding residual stresses in large-scale tubular K-joints', *Fatigue & Fracture of Engineering Materials & Structures* , doi: 10.1111/j.1460-2695.2012.01712.x, 2012.

[7] S. KOU: *Welding metallurgy*, John Willey and Sons, 2003.

[8] T. DEBROY and S. DAVID: 'Physical processes in fusion welding', Reviews of Modern Physics, Vol. 67, No. 1, pp. 85-112, 1995.

[9] T. ZACHARIA, J. VITEK, J. GOLDAK, T. DEBROY, M. RAPPAZ and H. BHADESHIA: 'Modeling of fundamental phenomena in welds', *Modelling Simul. Mater. Sci. Eng.*, Vol. 3, pp. 265-288, 1995.

[10] J.-M.. DREZET and S. MOKADEM: 'Marangoni convection and fragmentation in laser treatment', *Material Science Forum* Vol. 508, pp. 257-262, 2006.

[11] J. GOLDAK, A. CHAKRAVARTI AND BIBBY A new finite-element model for welding heat-sources. *Metall. Trans. B* , Vol. 15B, , No. 2, pp. 299–305, 1984.

[12] C. ACEVEDO: *Influence of Residual Stresses on Fatigue Response of Welded Tubular K-Joints,* thesis, Ecole Polytechnique Federale de Lausanne 5056, 2011.

[13] D. DEAN and M. HIDEKAZU: ' Prediction of welding residual stress in multi-pass butt-welded modified 9Cr–1Mo steel pipe considering phase transformation effects'. *Computational Materials Science* , Vol. 37, pp. 209–219, 2006.

[14] J. FRANCIS, H. BHADESHIA and P. WITHERS: 'Welding residual stresses in ferritic power plant steels, review', *Materials Science and Technology*, Vol. 23, No. 9, pp. 1009-1020, 2007.

[15] ISO 6507-1:1997: Metallic materials -- Vickers hardness test -- Part 1: Test method, 1997.

[16] N. KOPERNIKUS: *Ch.4. Classification of steels, welding of mild steels* Welding and Joining Institute, 2004.

[17] ABAQUS: *Analysis user's manual version 6.11*, Dassault Systèmes, 211.

[18] L.-E.. LINDGREN: 'Finite element modeling and simulation of welding Part 1: increased complexity', *Journal of Thermal Stresses*, Vol. 24, pp. 141-192, 2001.

[19] L. BORGES and A. NUSSBAUMER: 'Advanced numerical modelling of fatigue size effects in welded CHS K-joints', *12th International Symposium on Tubular Structures* (ISTS 12), Shanghai, 2008.

[20] A. SCHUMACHER, S. STRUM, S. WALBRIDGE, A. NUSSBAUMER and M. HIRT: *Fatigue design of bridges with welded circular hollow sections* . Report ICOM 489E, Swiss Federal Institute of Technology (EPFL), Lausanne, 2003.

[21] L. RAYMOND and J. CHIPMAN: 'Thermodynamic functions of iron', *J. Trans. Met. Soc. AIME*, Vol. 239, No. 1, pp. 630-633, 1967.

[22] V. PAPAZOGLOU and K. MASUBUCHI: 'Numerical analysis of thermal stresses during welding including phase transformation effects', *Journal of Pressure Vessel Technology* Vol. 104, pp. 198-203, 1982.
[23] B. SAINT-GERMAIN: *Etude expérimentale et numérique des distorsions de structures mécanosoudées*, thesis, Ecole Centrale Paris, 2006.
[24] EN1993 Part 1-2: Eurocode 3 Design of steel structures - Part 1-2, General rules - Structural fire design, Brussels, European Committee for Standardization, 2005.
[25] P. MICHALERIS: *Courses at the Pennsylvania State University*, 2011.
[26] P. DONG and J. HONG: *Recommendations for determining residual stresses in fitness-for-service assessment*, Welding Research Council Bulletin WRC, 2002.
[27] L.-E.. LINDGREN: 'Modeling for residual stresses and deformations due to welding- knowing what isn't necessary to know', In: Mathematical Modeliing of Weld Phenomena, 6, pp. 491-518, 2001.
[28] W.K.C. JONES and P.J. ALBERRY: 'A model for stress accumulation in steels during welding', *Metals Technology* Vol. 11, pp. 557-566, 1977.
[29] J. CARON, C. HEINZE, C. SCHWENK, M. RETHMEIER, S.S. BABU and J. LIPPOLD: 'Effects of continuous cooling transformation variations on numerical calculation of welding-induced residual stresses', *Welding Journal* Vol. 89, pp. 151-169, 2010.